JOURNAL OF SPACECRAFT AND ROCKETS
Vol. 38, No. 4, July–August 2001

Proton Spectra Detected by the Proton Switches on the CRRES Satellite

M. Cyamukungu* and G. Grégoire†
Université Catholique de Louvain, B-1348 Louvain-la-Neuve, Belgium
D. Heynderickx,‡ M. Kruglanski,§ and J. Lemaire¶
Belgian Institute for Space Aeronomy, B-1180 Brussels, Belgium
and
J. B. Blake** and R. S. Selesnick††
The Aerospace Corporation, Los Angeles, California 90009

A thorough detector characterization method is described and applied to analyze the data from the proton switches flown on the Combined Release and Radiation Effects Satellite (CRRES). The results are compared with the CRRESPRO model based on observations of the proton telescope (PROTEL), which was on board the same satellite. A general good agreement is observed at positions where the flux of high energy protons is low. In regions of harder proton spectra, the CRRESPRO fluxes are higher than those deduced from the proton switches data. One possible explanation for this discrepancy may be that high energy protons penetrating into the PROTEL detector through the side shielding may not have been properly accounted for.

Nomenclature

dA	=	effective element of the outer dome surface looking into $d\omega$, cm^2
$d\boldsymbol{\sigma}$	=	element of the outer dome surface, cm^2
$d\omega$	=	element of solid angle toward the $(1, \beta, \eta)$ direction, sr
E	=	particle energy, MeV
E_{th}	=	energy threshold for a given channel, MeV
E_u	=	upper particle energy limit for a given channel, MeV
$F_d(\omega)$	=	function describing the angular distribution of particles that hit the aperture surface S [1]
G	=	geometrical factor of the aperture surface S, cm^2 sr
$J(E_{\text{th}} < E < E_u)$	=	integral flux of particles with $E_{\text{th}} < E < E_u$, cm^{-2} sr^{-1} s^{-1}
$J_d(E)$	=	energy-dependent differential flux, cm^{-2} sr^{-1} s^{-1} MeV^{-1}
N	=	time averaged counting rate of a detector, s^{-1}
$p(E)$	=	intrinsic efficiency averaged over the detector solid angle Ω and the aperture surface S [1]
$Q(\omega)$	=	mean value of the intrinsic efficiency $q(\boldsymbol{\sigma}, \omega)$ averaged over a detector aperture surface S exposed to the proton flux for a given incidence direction (solid angle coordinates) [1]
$q(\boldsymbol{\sigma}, \omega)$	=	intrinsic efficiency averaged over the energy spectrum [1]
R	=	external radius of the spherical shield, cm
$\boldsymbol{r}$	=	unit vector in the direction of an incoming particle
S	=	dome outer surface, cm^2
XYZ	=	master coordinate system used to describe positions on the dome; the Z axis is oriented from the center of the dome basis toward the top; the X axis lies in the base plane and is perpendicular to Z; and the Y axis completes the right-handed orthogonal coordinate system
xyz	=	local coordinate system at a given position on the dome surface; the z axis is perpendicular to the dome surface, and the y axis lies in the meridian plan across the position on the dome surface, is perpendicular to z, and is oriented toward increasing θ angles. The x axis completes the right-handed orthogonal coordinate system
β	=	polar angle in the spherical coordinate system derived from xyz, rad
$\epsilon(E, \boldsymbol{\sigma}, \omega)$	=	intrinsic detection efficiency of a particle having energy E and impacting $d\boldsymbol{\sigma}$ through $d\omega$ [1]
η	=	azimuthal angle in the spherical coordinate system derived from xyz, rad
θ	=	polar angle in the spherical coordinate system derived from XYZ, rad
ϕ	=	azimuthal angles in the spherical coordinate system derived from XYZ, rad
$\phi_d(E, \omega)$	=	differential flux of particles, cm^{-2} sr^{-1} s^{-1} MeV^{-1}
Ω	=	total field-of-view solid angle, sr

Subscripts

i	=	subscript number for a property of channel i
j	=	subscript number for a property of detector j
obs	=	subscript indexing an experimental result

Received 30 August 2000; revision received 1 February 2001; accepted for publication 2 February 2001. Copyright © 2001 by the American Institute of Aeronautics and Astronautics, Inc. All rights reserved.

*Research Assistant, Institut de Physique Nucléaire, Chemin du Cyclotron 2.
†Professor, Institut de Physique Nucléaire, Chemin du Cyclotron 2.
‡Werkleider, Ringlaan 3.
§Research Assistant, Ringlaan 3.
¶Head of the Fundamental Dynamic Group, Ringlaan 3; also Professor, Institut d'Astronomie et de Géophysique "George Lemaître," Université Catholique de Louvain, Chemin du Cyclotron 2, B-1348 Louvain-la-Neuve, Belgium.
**Director, Space Particles and Fields Department, Space and Environmental Technology Center, P.O. Box 92957.
††Staff Member, Space Particles and Fields Department, Space and Environmental Technology Center, P.O. Box 92957.

Introduction

ON 25 July 1990, the Combined Release and Radiation Effects Satellite (CRRES) was launched into a 350 × 35,000 km,

18-deg inclination orbit. This paper reports on the proton spectral information measured by the proton switches (PS) along the CRRES orbit in the energy range 20–150 MeV. The analyzed data cover the quiet period from 22 August 1990 to 24 March 1991 and the active period from 25 March 1991 to 18 August 1991, during which a new proton belt was still present five months after the beginning of the 24 March 1991 magnetic storm. The terms "quiet" and "active" are used here for reference to the CRRES mission period before and following the 24 March 1991 storm, respectively.

Preliminary results along with rough approximations of the PS properties were presented in Ref. 1. The later results could not be used unrefined in a detailed spectrum characterization. Furthermore, the data set processed during the mentioned period appears to be of better quality, (i.e, no background count rate was observed outside the inner belt region during the quiet period) compared with the preliminary data acquired on 23 September 1990.

By comparison to the proton telescope (PROTEL) equipped with 24 energy channels,[2] the 4-channel PS system is very simple and as such it has the advantage of providing directly exploitable data for rough flux estimates. However, to be used for precise flux determination, such a simple detector needs to be thoroughly characterized. Indeed, because little redundant information may be expected from raw data, an optimal use of the output from each channel allows making up for their limited number. A large part of this study was devoted to a detailed evaluation of the PS system.

A description of this detector is presented, with details regarding the detector size along with the precise Monte Carlo calculation of the detection efficiency. The general formula relating counting rates to detector and flux properties is used to derive expressions of the counting rates generated by proton fluxes with a known angular distribution. In addition, the angular dependence of the PS efficiency is derived and serves to assess the characteristics of the proton angular distribution along the CRRES orbit. The proton spectra measured during the quiet period of the CRRES mission are presented and compared to the spectra derived by use of the AP-8 MAX and CRRESPRO models. The PS active-period spectra are derived and compared to the quiet-period ones and to the results from the mentioned models.

Description of the PS System

Instrument Setup

The PS system is made of two sensors, PS1 and PS2. Each of them is an assembly of a cubic silicon detector supported by a Mallory 1000 disk (90% W–nickel–copper) and shielded by an aluminum dome. The two sensors differ only in the thickness of the shielding dome. For each, the electronic readout has two threshold energies set to 5 MeV ("L" channels) and 7 MeV ("H" channels), which defines the four PS channels named hereafter 1L, 1H, 2L, and 2H. A cut view of the PS mechanical model used for the Monte Carlo simulation is shown in Fig. 1. The sizes of the main elements of this detector are, first, the aluminum spherical shield has a 5.15-mm inner radius and a 7.25-mm outer radius for the PS2. The outer radius of the PS1 is 16.6 mm. Second, the lithium drifted silicon detector is a cube with a 3-mm edge, located at the center of the spherical shield. Finally, the back side of the PS consists of 3 mm of Mallory 1000, 1.2 cm of copper, and then the entire CRRES spacecraft. The shielding effect of these mallory and copper plates is equivalent to ≈5-cm-thick aluminum. The spacecraft was massive for shielding purposes but, of course not uniform. A simulation based on an isotropic proton flux and a total of 8-cm-thick 1×1 m aluminum back side shielding has shown that no back side protons were detected for proton energies up to 150 MeV. The change of detection efficiency mainly due to protons with higher energies (up to 500 MeV) at normal incidence on the backplate did not exceed 1% of the value obtained for 150 MeV protons. Therefore, during the final efficiency calculations, no particle coming from the back side of the PS was initiated.

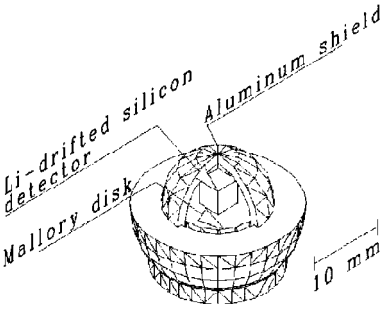

Fig. 1 Schematic representation of the PS model.

General Calculation of the Detection Efficiency

The availability of simulation tools has led charged particle detector designers and users to perform the thorough characterizations needed for spectrum determination. An example of such an extensive use of a Monte Carlo method in detector characterization may be found in Ref. 3.

As part of the set of detector properties, the intrinsic efficiency, defined as the ratio of the number of particles that hit the sensitive element to the number of particles that reach the detector aperture, is a useful complement to the usually used geometrical factor. The efficiency functions defined in this section will be presented using the following counting rate expressions. The time-averaged counting rate of a one-particle species detector is expressed as[4]

$$N = \int_S \mathrm{d}A \int_\Omega \mathrm{d}\omega \int_{E_{\mathrm{th}}}^{E_u} \epsilon(E, \boldsymbol{\sigma}, \omega)\phi_d(E, \omega)\,\mathrm{d}E \qquad (1)$$

where (see Appendix) the element of solid angle $\mathrm{d}\omega = \sin\beta\,\mathrm{d}\beta\,\mathrm{d}\eta$, and the effective element of the dome area looking into this solid angle $\mathrm{d}A = \mathrm{d}\boldsymbol{\sigma}\cdot\boldsymbol{r} = \sin\theta\cos\beta\,\mathrm{d}\theta\,\mathrm{d}\phi$.

Usually, the assumption made is that the differential flux may be expressed as $\phi_d(E, \omega) = J_d(E)F_d(\omega)$, a product of the energy differential flux $J_d(E)$ and the angular dependence $F_d(\omega)$. Using the general counting rate expression in Eq. (1), precise deconvoluted spectra characterizing both the energy and the angular dependence may be obtained if the detector system has a sufficient number of energy channels and several sensors pointing in different directions.

In the case of simple detectors with a limited number of fields of view, no precise angular dependence of the particle flux may be obtained from the detector data. In such a case, the angular distribution is, rather, assumed, and the deconvolution of the energy spectrum may be performed. Likewise, for detectors with a limited number of energy channels, the angular distribution of particles may be derived if an energy spectrum is assumed. The methods to be used in the case of known or assumed energy or angular distribution of particle fluxes are described later.

Deconvolution of Angular Distributions

If the energy spectrum is known or assumed, an averaged intrinsic efficiency may be defined as

$$q(\boldsymbol{\sigma}, \omega) = \frac{\int_{E_{\mathrm{th}}}^{E_u} \epsilon(E, \boldsymbol{\sigma}, \omega)J_d(E)\,\mathrm{d}E}{\int_{E_{\mathrm{th}}}^{E_u} J_d(E)\,\mathrm{d}E} \qquad (2)$$

Thus, the counting rate in channel i of sensor j for this energy spectrum may be expressed as

$$N_{\mathrm{ji}} = J(E_{\mathrm{th}} < E < E_u) \int_{\Omega_j} F_d(\omega)\left[\int_{S_j} q_{\mathrm{ji}}(\boldsymbol{\sigma}, \omega)\,\mathrm{d}A_j\right]\mathrm{d}\omega \qquad (3)$$

The integral in brackets may be expressed also as

$$Q_{\mathrm{ji}}(\omega) = \frac{1}{A_j}\int_{S_j} q_{\mathrm{ji}}(\boldsymbol{\sigma}, \omega)\,\mathrm{d}A_j \qquad (4)$$

The counting rate expression is thus

$$N_{\mathrm{ji}} = J(E_{\mathrm{th}} < E < E_u) \int_{\Omega_j} F_d(\omega)Q_{\mathrm{ji}}(\omega)A_j(\omega)\,\mathrm{d}\omega \qquad (5)$$

The parameters of the angular distribution appearing in Eq. (5) are accessed if the product $Q_{\mathrm{ji}}(\omega)A_j(\omega)$ is not constant over the detector aperture field of view. Otherwise, the number of detectors

characterized by different values of the QA product must be at least equal to the number of parameters of the angular distribution model, $F_d(\omega)$. Of course, detectors with sensitive elements on their aperture working in coincidence with a common central sensor or rapidly spinning satellites are alternative solutions to increasing the number of angle channels and making possible the deconvolution of the angular distribution.

Deconvolution of Energy Spectra

Given the angular dependence $F_d(\omega)$, the intrinsic efficiency averaged over the detector solid angle Ω and the aperture surface S is expressed as

$$p(E) = \frac{\int_S \int_\Omega \epsilon(E, \boldsymbol{\sigma}, \omega) F_d(\omega)\, \mathrm{d}A\, \mathrm{d}\omega}{\int_S \int_\Omega F_d(\omega)\, \mathrm{d}A\, \mathrm{d}\omega} \tag{6}$$

where the integral in the denominator is equal to G. Therefore, using Eqs. (1) and Eqs. (6), the counting rate of channel i of a detector sensor j is given by

$$N_{\mathrm{ji}} = G \int_{E_{\mathrm{th}}}^{E_u} p_{\mathrm{ji}}(E) J_d(E)\, \mathrm{d}E \tag{7}$$

To be extracted, the information on the energy spectrum contained in Eq. (7) must be significantly modulated by the function $p_{\mathrm{ji}}(E)$, especially when the detector is made of few energy channels.

Application to the PS

Angular Dependence of the PS Efficiency

The sensitivity of the PS to the angular distribution of the proton flux was evaluated for typical energy spectra $J_d(E) = J_{d0}(E/E_0)^{-\gamma}$ with $\gamma = 3$ and 2, two typical power law indexes obtained by fitting AP-8 spectra. The energy value $E_0 = 50$ MeV and $J_{d0} = J_d(E_0)$. The simulation procedure using the GEANT version 3.21 software[5] was as follows: The detector dome was considered as inscribed in a square lying on a plane that passes across the center of the dome (Fig. 2). The incident proton momentum was perpendicular to this plane from the hemisphere facing the PS detector. The proton initial positions were on the dome, but generated so that their density over the square was uniform. The effective surface of the dome facing the proton "beam" was calculated and used to evaluate the product of $Q(\omega)$ (the average efficiency defined as the number of hits registered by the sensor to the total number of events initiated on the dome) and A (the effective surface) from Eq. (4). The products QA are shown in Fig. 3. It can be seen that these products are almost constant over the detector field of view for the considered energy spectra and at two azimuthal angles. In fact, the sensors were designed to have as weak an efficiency dependence upon angle of incidence as possible. Therefore, the angle-dependent counting rate is expressed as in Eq. (5):

$$N_{\mathrm{ji}} = C \int_\Omega F_d(\omega)\, \mathrm{d}\omega \tag{8}$$

that is, the product of a constant $C = J(E_{\mathrm{th}} < E < E_u) Q(\omega_0) A(\omega_0)$ (ω_0 is any incidence solid angle within the 2π field of view) and the integral over the whole field of view of the angular part of the differential flux. The angular density function, $F_d(\omega)$, may be decomposed into an isotropic term and a pure pitch angle-dependent function of the form $H_d(\omega) = H_d(\alpha) = f(\sin\alpha)$. It can be demonstrated that such an angular distribution, having a center of symmetry, does not induce angular-dependent counting rates in a 2π field-of-view detector. The counting rates detected by 2π field-of-view sensors are angular dependent if the angle-dependent density function of the flux is asymmetric either under rotation around the magnetic field direction or under reflection in a plane perpendicular to the magnetic field. Such asymmetric angular distributions are usually observed in low-altitude regions where east–west asymmetry of fluxes or particle precipitation into the atmosphere occur.

The CRRES was spinning with a period of 30 s. Because the PS sampling period is much shorter than the CRRES rotation period, it is possible to gather information on the proton flux anisotropy. In particular, the counting rate dependence on the sensor orientation shown in Fig. 4 indicates that the angular distribution over the whole 4π solid angle is not centrosymmetric. (The dashed line in Fig. 4 is a Gaussian fit of the data that were used to correct the counting rate for the monotonically increasing average flux within the 30-s time interval delimited by dotted lines.) On the other hand, an examination of the smooth counting rate variation on a lower scale (following a 48-deg rotation angle) indicates that the angular distribution scanned by the 2π detector field of view during the 4-s sampling period is almost isotropic. However, the pertinence of this approximation may be assessed only on the basis of the resulting uncertainties on the other parameters characterizing the proton spectra. On the basis of the PS properties described here, it is seen that the resolution of a detailed pitch angle distribution is beyond the PS capabilities.

PS Response to Proton Fluxes

In our attempt to extract spectral information from the PS, an isotropic proton flux was assumed over the detector field of view along the CRRES orbit. Also, as already mentioned, it was assumed that no proton could reach the sensor from the back of the detector. In such conditions, the value of the constant appearing in Eq. (7) is $G = \frac{3}{2}(\pi R)^2$ (see Appendix).

The energy dependence of the detection efficiencies for each PS channel was calculated using the Centre Européen de Recherche Nucléaire (CERN) Monte Carlo code GEANT version 3.21. These detection efficiencies are shown in Fig. 5. The products of the geometrical factor G by the mean values of the efficiency functions averaged over the covered energy ranges are shown in Table 1 for comparison with the values given in Ref. 1. The latter have been multiplied by 2π for conversion into cm^2 sr units. Such values, defined as mean energy-dependent geometrical factors of the PS channels, may be used in rough estimates of counting rates in regions where flat energy spectra over the channel energy range are encountered. The upper limit of an energy interval was determined so that the ratio of the efficiency integral over this interval was 95% of the total

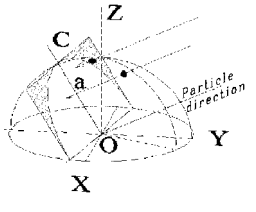

Fig. 2 Simulation setup for the calculation of the QA product.

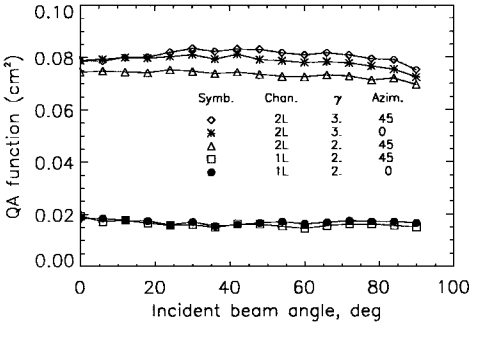

Fig. 3 Product QA as a function of angles θ and ϕ, and the power law index γ of the proton spectrum.

Table 1 PS energy ranges and average geometrical factors

	This work		Ref. 1	
Channel	Energy range, MeV	Average geometrical factor, cm^2 sr	Energy range, MeV	Average geometrical factor, cm^2 sr
1L	52–118	0.209	51–107	0.226
2L	21–102	0.223	21–84	0.245
1H	52–91	0.188	51–77	0.170
2H	22–71	0.211	23–51	0.163

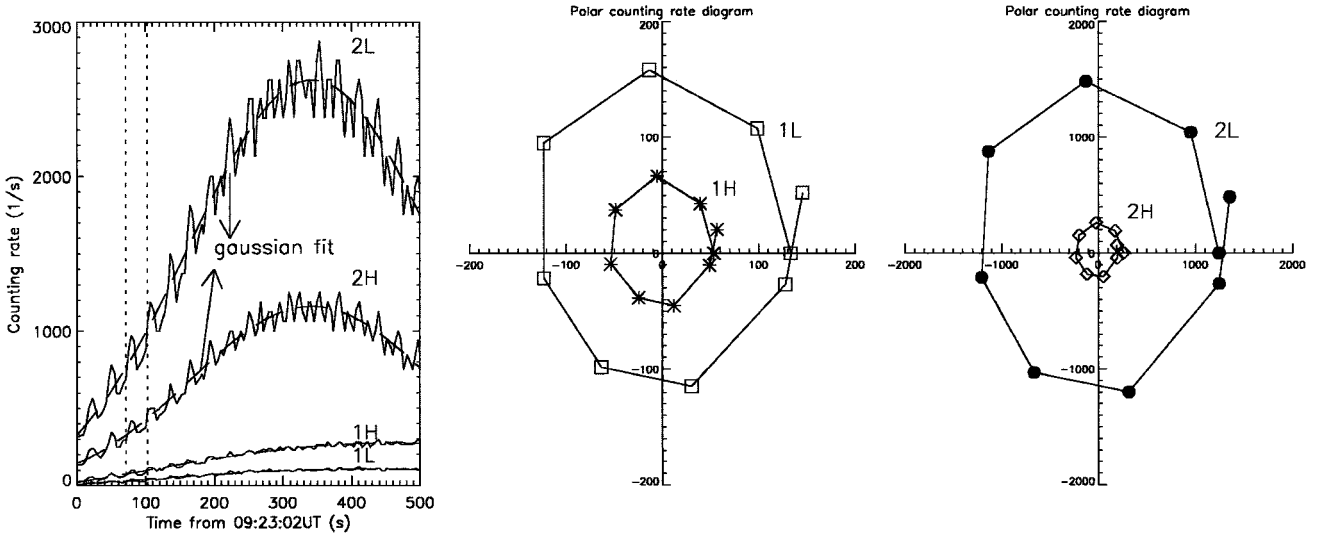

Fig. 4 Time (Cartesian diagram) and angular (polar diagrams) dependence of the counting rate of the four PS channels, as observed on 23 August 1991 at about 5182-km altitude, 13.45° latitude, 55.1° longitude, $L = 1.82$.

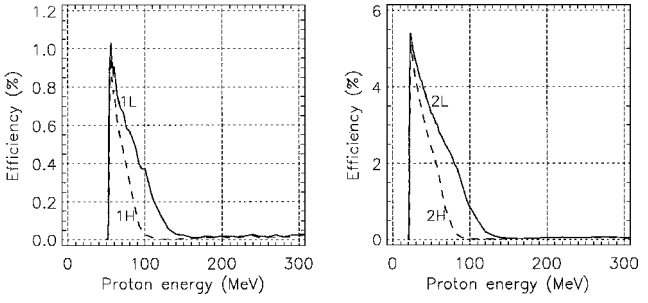

Fig. 5 Proton detection efficiency of the PS channels (2L, 2H, 1L, and 1H) when no particle is supposed to reach the detector from the back side.

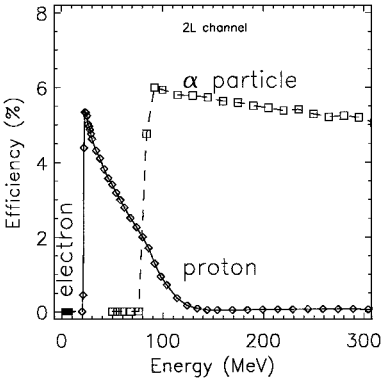

Fig. 6 Detection efficiency of electrons, protons, and α particles by the PS.

integral over the energy, ranging from the threshold to 150 MeV (the highest energy significantly detected by the PS). It is generally admitted that the accuracy of the actual stopping power and energy loss codes is around 10%. Thus, the values in Table 1 are considered to be in good agreement, given the totally different methods used to evaluate the energy ranges and geometrical factors.

PS Sensitivity to Electrons and α Particles

In addition to their effects in the determination of the detection efficiency of protons, the shielding and the electronic thresholds play a key role in providing the PS with very low electron and α particle efficiencies. The detection efficiencies for isotropic fluxes of electrons and α particles (also calculated using the GEANT 3.21 code) are shown in Fig. 6 as a function of energy. The detection efficiency of electrons is less than 10^{-6} up to 10 MeV, showing that almost no single electron will be counted in the PS channels. The setting of the lowest electronic threshold to 5 MeV, which is about 10 times higher than the mean electron energy loss in the silicon detector, reduced considerably the probability of electron counting due to signal pileup. This fact is also demonstrated by the zero counting rate observed in the outer radiation belt at $L > 4$.

The average detection efficiency was used to quantify the level of contamination of the PS channel 2L by α particles. An integral omnidirectional flux of $J(E > 80\ \text{MeV}) \approx 1\,p/(\text{s sr cm}^2)$ is the threshold level that induces one count in the 2L channel during the 4-s integration time. This threshold level is not so high an α particle flux value, and one may fear that at some positions along the CRRES orbit, the PS 2L channel may be contaminated by α particles. However, we know that the Cosmic Ray Albedo Neutron Decay (CRAND) source only injects protons. The threshold α particle flux for channel 1L is $J(E > 200\ \text{MeV}) \approx 2\,p/(\text{s sr cm}^2)$. Because of this rather high threshold level, one is led to consider this channel and the 1H channel, which has the same energy threshold, as far less α contaminated. The analyzed data were filtered on the criterion that the corresponding counting rates of all the channels were greater than zero, which ensures that only proton dominated counting rates were taken into account. In fact, as a result of this selection, only data from regions near the heart of the belt were kept during the quiet period. For the active period, the selected data belong to the "old" and the "new" belt and to a particle burst observed around 10 June 1991 near $L = 4$.

Proton Spectra During the Quiet Period

The available quiet-period data cover the time intervals from 21 August 1990 to 20 December 1990 and from 19 February 1991 to 23 March 1991. Counting-rate values averaged over $(B/B_0, L)$ bins of 0.01- and 0.05-R_E width in B/B_0 and L, respectively, were used to determine the power law parameters by minimizing the function $F(J_{d0}, \gamma)$ defined as

$$F(J_{d0}, \gamma) = \sum_{j=1}^{2} \sum_{i=1}^{2} \frac{(N_{\text{ji}} - N_{\text{ji-obs}})^2}{N_{\text{ji-obs}}} \tag{9}$$

where N_{ji} is given by Eq.(7).

The differential energy spectra derived by this least-squares-fit method were integrated over the PS energy channels, and the results were compared to AP-8 MAX predictions. The general feature of the proton spectra is that the absolute value of the differences between the PS and AP-8 MAX results are less than 50% of AP-8 MAX predictions for positions where $1.2 < L < 1.5$ and $B/B_0 < 2$.

Afterward, counting rates acquired in the equatorial region $(1 < B/B_0 < 1.0001)$ were selected and averaged over 0.05-R_E-width L bins. The differential spectra derived by least-squares fit of these data were integrated over the CRRESPRO channel 16 (energy range 40.2–43.2 MeV),[6] and the results were divided by 3 MeV.

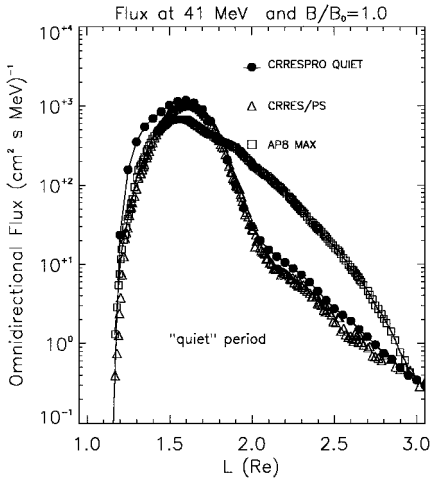

Fig. 7 Comparison between the CRRES/PS, CRRESPRO QUIET, and AP-8 MAX proton equatorial fluxes at 41 MeV as a function of *L*.

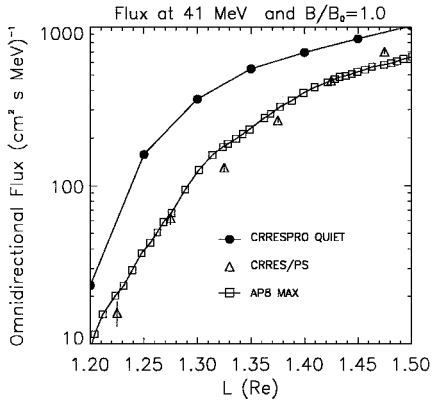

Fig. 8 Detailed view of fluxes in the $1.2 < L < 1.5$ region.

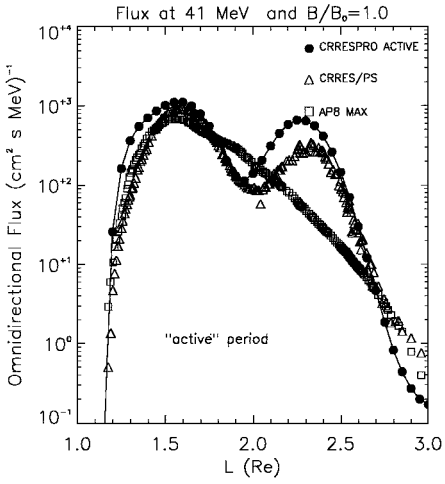

Fig. 9 Comparison between the CRRES/PS, CRRESPRO ACTIVE, and AP-8 MAX proton equatorial fluxes at 41 MeV as a function of *L*.

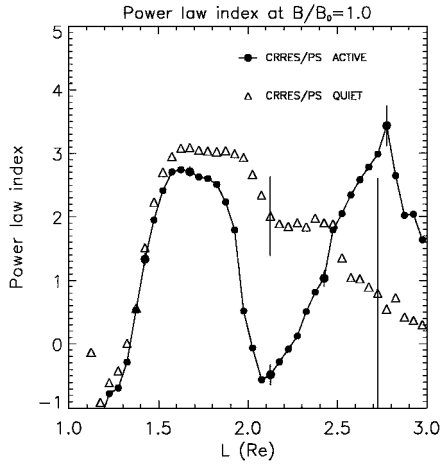

Fig. 10 Equatorial power law indexes valid for the energy range 20–150 MeV.

The resulting omnidirectional fluxes are shown in Fig. 7 and have been compared to the NASA model AP-8 MAX and to the CRRESPRO QUIET model, based on the fluxes measured during the quiet period on board the CRRES using PROTEL. In the $L < 1.5$ region, the AP-8 MAX equatorial fluxes tend to be systematically higher than the PS results, but this discrepancy is in general lower than 50%, as shown in Fig. 8. This relatively fair agreement between AP-8 MAX and the actual results has been observed already[7,8] and is ascribed to the stability of magnetospheric properties at the inner edge of the inner radiation belt, contrarily to the outer edge, in which the measured fluxes are very sensitive to the space weather. The AP-8 trend to the overestimation of equatorial proton fluxes below 100 MeV, at $L = 1.4$, has also been observed on the basis of Solar, Anomalous, and Magnetospheric Particle Explorer/Proton/Electron Telescope (SAMPEX/PET) data acquired in solar minimum-activity conditions.[9] However, the discrepancy observed in such conditions is more marked: The differences between AP-8 MIN and the model derived from the SAMPEX/PET data sometimes amount to an order of magnitude.

For the $L > 1.5$ region, a good agreement is found between the PS results and the CRRESPRO QUIET predictions.[7] The proton flux is underestimated by AP-8 MAX for $1.5 < L < 1.8$, and overestimated for $L > 1.8$, as indicated in Fig. 7.

Proton Spectra During the Active Period

The same procedure as the one already described was used to deduce the parameters of the proton spectra during the active period. The fluxes of 41-MeV protons derived from the PS data are shown in Fig. 9 and compared to the results from AP-8 MAX and CRRESPRO ACTIVE models. At $L < 1.5$, no difference is observed between the fluxes acquired during the quiet and the active periods. In other words, the spectra detected by the PS in this region were not significantly affected by the ambiant geomagnetic conditions and the new belt that appeared at $2 < L < 2.5$ after the 24 March 1991 storm. The agreement between the PS and CRRESPRO for higher L values (observed during the quiet period) does not hold any more, except in a thin region between $L = 1.6$ and 2.0 and around $L = 2.7$.

The good agreement found between CRRESPRO QUIET and the PS results at higher L values indicates that both instruments are reliable and well characterized for the CRRES quiet conditions in this region. Moreover, the spectral information (J_{d0} and γ) obtained from the PS are considered as describing the actual proton spectra along the CRRES orbit, because the statistical uncertainties (of which typical values have been plotted as error bars in Fig. 10) on each of the parameters are rather low. This result not only validates our hypothesis on the flux isotropy over the detector field of view, but it also validates the use of these parameters to investigate the changes that affected the proton spectra after 24 March 1991. The power law indexes for the quiet and active periods are shown in Fig. 10.

According to the observed power law index, the active period is mainly characterized by 1) an injection of high-energy protons within the region $2 < L < 2.5$ ($\gamma < 2$); 2) an increase of the high-energy contents of the proton flux at $1.6 < L < 2.0$, but with a power law index $\gamma > 2$; and 3) a hard proton spectrum at $L < 1.5$ and $L > 3$ ($\gamma < 2$).[10]

As a matter of fact, the discrepancy between the CRRESPRO and the PS results appears to be higher at positions where $\gamma < 2$. This fact may indicate that this discrepancy results from a possible contamination of the PROTEL data by high-energy protons abundant where $\gamma < 2$ but unaccounted for in the geometrical factor calculation and contamination correction.[6]

Conclusions

We have shown throughout this paper that a simple but well-characterized detector may give valuable results to complement the output from more sophisticated instruments. A more important fact, from the instrumental point of view, is that the absence of contamination of the PS results by electrons allowed the measurement of proton fluxes that may be confidently compared to the existing models. From other such comparisons, including as many instruments as possible, one may draw a map of space regions where the same values of proton fluxes have been measured by different instruments. In particular, the agreement (within a 50% precision) between observed proton fluxes and AP-8 predictions at the inner edge of the proton radiation belt should be further investigated. If the existence of such stable and well-modeled regions is demonstrated, the fluxes there might be considered as reference values to use for in-flight (inter)calibration of detectors.

Appendix: Calculation of the Geometrical Factor of the PS Dome

We have noted in this paper that the product of the geometrical factor of a detector aperture and the intrinsic detection efficiency relates the counting rates to particle flux. In this Appendix, the geometrical factor of a hemispheric dome is calculated. The coordinate system used here is represented in Fig. A1. We consider first a particle impacting the surface element $d\boldsymbol{\sigma}$ of a dome having a radius R, from the solid angle $d\Omega$.

The spherical coordinates of the surface element in the dome coordinate system (XYZ) are (R, θ, ϕ). The components of the particle momentum are expresssed by use of $(1, \beta, \eta)$ in the local coordinate system (xyz). The components of the particle momentum in the dome coordinate system are obtained using the transformation matrix M expressed as

$$M = \begin{bmatrix} \cos\phi & \sin\phi\cos\theta & \sin\phi\sin\theta \\ -\sin\phi & \cos\phi\cos\theta & \cos\phi\sin\theta \\ 0 & -\sin\theta & \cos\theta \end{bmatrix} \tag{A1}$$

We are particularly interested by the components of the momentum for particles coming from the half-hemisphere that contains the dome, because as a result of the shielding of the dome by the back side satellite body, only such particles may reach the sensor and be counted.

Particles coming from the dome hemisphere are characterized by a negative Z component of their momentum, that is

$$\cos\theta_0 = -\sin\theta\sin\beta\sin\eta + \cos\theta\cos\beta \le 0 \tag{A2}$$

which is equivalent to a local polar angle β that satisfies the equation

$$\tan\beta \le 1/\tan\theta\sin\eta \tag{A3}$$

Introducing this condition into the general expression of the geometrical factor, G, one gets

$$G = \int_S\int_\Omega F_d(\omega)\,\mathrm{d}A\,\mathrm{d}\omega = \int_{\phi=0}^{2\pi}\int_{\eta=0}^{2\pi}\int_{\theta=0}^{\pi/2}\int_{\beta=0}^{\beta_0} R^2 F_d(\beta,\eta)\sin\beta\sin\theta\cos\beta\,\mathrm{d}\beta\,\mathrm{d}\theta\,\mathrm{d}\eta\,\mathrm{d}\phi \tag{A4}$$

where the element of solid angle $\mathrm{d}\omega = \sin\beta\,\mathrm{d}\beta\,\mathrm{d}\eta$, and the effective element of the dome area looking into the solid angle $\mathrm{d}\omega$, $\mathrm{d}A = d\boldsymbol{\sigma}\cdot\boldsymbol{r} = \sin\theta\cos\beta\,\mathrm{d}\theta\,\mathrm{d}\phi$. $\beta_0 = \arctan(1/\tan\theta\sin\eta)$ is the upper limit of the integral over the variable β.

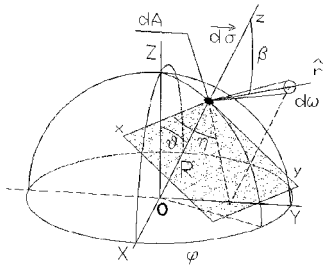

Fig. A1 Coordinate system used in the evaluation of the dome geometrical factor.

Looking at the local coordinate (β, η), one notices that the limit of the integral over the variable β is β_0 when $0 \le \eta < \pi$, whereas it is $\pi/2$ for $\pi/2 \le \eta < 2\pi$. Thus, for isotropic fluxes, $F_d(\omega) = 1$ and the geometrical factor is given by

$$G = G_{\eta<} + G_{\eta>} \tag{A5}$$

where

$$G_{\eta<} = \int_{\phi=0}^{2\pi}\int_{\eta=0}^{\pi}\int_{\theta=0}^{\pi/2}\int_{\beta=0}^{\beta_0} R^2\sin\beta\sin\theta\cos\beta\,\mathrm{d}\beta\,\mathrm{d}\theta\,\mathrm{d}\eta\,\mathrm{d}\phi \tag{A6}$$

$$G_{\eta>} = \int_{\phi=0}^{2\pi}\int_{\eta=\pi}^{2\pi}\int_{\theta=0}^{\pi/2}\int_{\beta=0}^{\pi/2} R^2\sin\beta\sin\theta \times \cos\beta\,\mathrm{d}\beta\,\mathrm{d}\theta\,\mathrm{d}\eta\,\mathrm{d}\phi = (\pi R)^2 \tag{A7}$$

The integral in Eq. (A6) may be simplified to

$$G_{\eta<} = \pi R^2\int_{\eta=0}^{\pi}\int_{\theta=0}^{\pi/2}\sin\theta\sin^2\beta_0\,\mathrm{d}\theta\,\mathrm{d}\eta = \frac{1}{2}(\pi R)^2 \tag{A8}$$

Using Eqs. (A7) and (A8), one gets the expression used as $G = G_{\eta<} + G_{\eta>} = \frac{3}{2}(\pi R)^2$.

Acknowledgments

The characterization of the PS, along with the analysis of the CRRES/PS data, were undertaken to check the data analysis methodology devised for the charged particle detector (CPD) on board the Ørsted satellite (PRODEX-ESA-SSTC Contract 170724). Work at The Aerospace Corporation was supported by the U.S. Air Force under Contract FP4701-93-C-0094. The authors thank P. Bühler for valuable discussions on the PS observations, including some comparison with STRV/REM data. Also, they are grateful for the constructive and very useful comments from the reviewers.

References

[1]Blake, J. B., and Imamoto, S. S., "Proton Switches," *Journal of Spacecraft and Rockets*, Vol. 29, No. 4, 1992, pp. 595, 596.

[2]Violet, M. D., Lynch, K., Redus, R., Riehl, K., Boughan, E., and Hein, C., "Proton Telescope (PROTEL) on the CRRES Spacecraft," *IEEE Transactions on Nuclear Science*, Vol. 40, No. 2, 1993, p. 242.

[3]Bühler, P., Ljungfelt, S., Mchedlishvili, A., Schlumpf, N., Zehnder, A., Adams, L., Daly, E., and Nickson, R., "Radiation Environment Monitor," *Nuclear Instruments and Methods in Physics Research A*, Vol. 368, No. 3, 1996, pp. 825–831.

[4]Sullivan, J. D., "Geometrical Factor and Directional Response of Single and Multi-Element Particle Telescopes," *Nuclear Instruments and Methods*, Vol. 95, No. 1, 1971, pp. 5–11.

[5]*GEANT Version 3.21/05*, CERN Program Library Office, Geneva, 1996.

[6]Meffert, J. D., and Gussenhoven, M. S., "Phillips Laboratory Space Physics Division Radiation Models: CRRESPRO DOCUMENTATION," PL-TR-94-2218, Environmental Research Papers, No. 1158, July 1994.

[7]Gussenhoven, M. S., Mullen, E. G., and Brautigam, D. H., "Philips Laboratory Space Physics Division Radiation Models," *Radiation Belts: Models and Standards*, Geophysical Monograph, edited by J. F. Lemaire, D. Heynderickx, and D. N. Baker, Vol. 97, No. 1, American Geophysical Union, Washington, DC, 1996, pp. 93–101.

[8]Cyamukungu, M., Lippens, C., Adams, L., Nickson, R., Boeder, C., Pierrard, V., Daly, E., Grégoire, GH., and Lemaire, J., "Magnetic Storm Acceleration of Radiation Belt Electrons Observed by the Scintillating Fibre Detector (SFD) on Board EQUATOR-S," *Annales Geophysicae*, Vol. 17, No. 12, 1999, pp. 1622–1625.

[9]Heynderickx, D., Kruglanski, M., Pierrard, V., Lemaire, J., Looper, M. D., and Blake, J. B., "A Low Altitude Trapped Proton Model for Solar Minimum Conditions Based on SAMPEX/PET Data," *IEEE Transactions on Nuclear Science*, Vol. 46, No. 6, 1999, pp. 1475–1480.

[10]Mullen, E. G., Gussenhoven, M. S., Ray, K., and Violet, M., "A Double-Peaked Inner Radiation Belt: Cause and Effect as Seen on CRRES," *IEEE Transactions on Nuclear Science*, Vol. 38, No. 6, 1991, p. 1713.

A. C. Tribble
Associate Editor